THE ASTROPHYSICAL JOURNAL, 563:673–686, 2001 December 20

A FILAMENT BETWEEN GALAXY CLUSTERS A3391 AND A3395

ERIC R. TITTLEY AND MARK HENRIKSEN
Joint Center for Astrophysics, University of Maryland, Baltimore County, Baltimore, MD 21250; etittley@jca.umbc.edu, mark@jca.umbc.edu
Received 2001 April 27; accepted 2001 August 21

ABSTRACT

Filamentary gas spanning the region between the galaxy clusters Abell 3391 and Abell 3395 has been detected using *ASCA* and *ROSAT* archived data. The gas has a minimum flux of 1.3×10^{-12} ergs cm^{-2} s^{-1} (0.8–10 keV). Within this filament resides a galaxy group for which a flux of $(2.0 \pm 0.3) \times 10^{-13}$ ergs cm^{-2} s^{-1} (0.8–10 keV) is determined. An analysis using ray-tracing determines light scattered into the filamentary region contributes 13% of the count rate. The structure in which the filamentary gas resides is postulated to be a filament aligned nearly lengthwise with the line of sight. Identification of this structure as a filament is based on the angular and redshift distribution of surrounding galaxies and clusters. The distribution is compatible with the structure being a quasi-linear structure tilted to the line of sight such that the ratio of the depth to the tangential distance is between 6:1 and 18:1. The filamentary gas contains on the order of 10^{13} $M_\odot$ of gas, which is close to 2% of the total mass of the system.

Subject headings: galaxies: clusters: individual (A3391, A3395) — large-scale structure of universe — X-rays: diffuse background — X-rays: galaxies: clusters

1. INTRODUCTION

It may be the case that the majority of the baryonic material in the universe has not been observed. Numerical simulations suggest that for a Λ CDM universe, a large fraction (up to $\frac{1}{2}$) remains in the intercluster medium, located in a hot (0.01–1 keV) but tenuous ($\sim \Omega_b \rho_c$) gaseous phase (Cen & Ostriker 1999). According to these same simulations, this gas is not located uniformly dispersed between the clusters of galaxies but is located, along with the gravitationally dominant dark matter and a significant fraction ($\sim \frac{1}{4}$) of the galaxy population, in weblike structures composed of filaments and, perhaps, sheets. Consequently, a large fraction of the baryon content of the universe, as inferred from primeval nucleosynthesis arguments, may yet to be observed. There is some disagreement, however, as to what fraction actually is observed. Cen & Ostriker (1999) claim only 20%, while the summation of Fukugita et al. (1998) accounts for more than 50% and finds 100% to be within the range given by the substantial errors. The accounting of Fukugita et al. (1998) argues that two-thirds of the baryonic material is in plasmas in groups of galaxies, based on scaling arguments from clusters. Hence the largest contribution is based on extrapolation rather than direct observation.

There is observational evidence for a large reservoir of low-density gas from the detection of O VI absorption in QSO spectra by intervening matter. Tripp et al. (2000) set an approximate lower limit of $\Omega_b(\mathrm{O\ VI}) > 0.005\ h_{65}^{-1}$ from Space Telescope Imaging Spectrograph (STIS) detections of four O VI absorbing systems. This is a sufficient density to reconcile the apparent deficit of observed baryonic material with the primeval nucleosynthesis predictions.

Briel & Henry (1995) reported the results of a search of the *ROSAT* All-Sky Survey for X-ray emission from filaments. The authors failed to find any and consequently put an upper limit on the electron density of filaments of $6 \times 10^{-5}\ h_{65}^{1/2}$ cm^{-3}, assuming a gas temperature of 1 keV. Examining the cosmic microwave background decrement, Campos et al. (1999) claim that a linear arrangement of galaxies and QSOs at $z = 2.5$ could represent a filament, with an observed decrement a result of the Sunyaev-Zeldovich effect from the filamentary gas. Scharf et al. (2000) claim that X-ray emission from a filament of galaxies has been detected in *ROSAT* data. The emission was found in one field from a sample of 22 deep exposures taken from the archives. The count rate is 2–3 σ above the background.

The best candidate for filamentary emission between clusters reported in the literature is given in Kull & Böhringer (1999). They find excess emission between the clusters A3562, A3558, and A3556 in the Shapley supercluster, as observed by the *ROSAT* Positive Sensitive Proportional Counter (PSPC). Scharf et al. (2000), however, note that the emission may be from gas ejected from the clusters during a merger. In such a case, the gas would not represent infalling filamentary gas. Some of the emission is coincident with two galaxy groups, but there exists a diffuse component that permeates the linear arrangement of clusters and groups. The structure spans 3.°8, or 13 h_{65}^{-1} Mpc. The gas unassociated with the principal clusters and groups, though difficult to separate from the principal component and any uncataloged galaxy groups, has a luminosity of $L_X = 3 \times 10^{43}$ ergs s^{-1}, a temperature $T < 1$ keV, and an electron density of $n_e = 5 \times 10^{-5}$ cm^{-3}. This fraction of the gas comprises approximately 10% of the total gas mass of the system.

Hot gas outside a cluster system has been reported around A2125 (Wang et al. 1997) from *ROSAT* PSPC observations. The gas either may be primordial or may have been ejected from the system during its formation. It is neither filamentary nor intracluster (it surrounds the host cluster), but it does have the characteristics expected for filamentary gas, providing an observational benchmark. They report a temperature of 0.85 ± 0.4 keV and an X-ray luminosity of 2.4×10^{43} ergs s^{-1}.

Other than accounting for the baryons, there is good reason to search for this gas. The state of the intergalactic medium in groups of galaxies is more sensitive to the nongravitational processes that occur in the system than in larger galaxy clusters (see Renzini 1997, for example). This sensitivity suggests that galactic evolution should strongly influence the gas in groups and, by extension, their even lower density counterparts, filaments. Even though fila-

ments likely have a lower fraction of their mass in galaxies, they also have a lower binding energy and so would be more sensitive to entropy changes. Markevitch (1999) proposes using the large cluster filament in Aquarius to study early star formation, suggesting that metal abundances may be extracted by performing a differential X-ray Gunn-Peterson test.

Filaments as structures are interesting as tests of structure formation theory. The physical process that leads to filaments has been the focus of considerable attention. Bond et al. (1996) note that the filamentary structure is present at early times in the initial density fluctuations. The peaks in the initial density field collapse first and form the largest objects at the scale over which the local density field is measured. This intuitively simple picture forms the basis of hierarchical clustering. Extending the picture, Bond et al. (1996) claim that it is alignment of the tidal tensors between nearby objects that leads to filamentary structure between the objects. Larger objects influence larger scales and produce larger filaments. Furthermore, a result of peak-patch theory (Bond & Myers 1996) is the preferential alignment of the tidal tensors of nearby density peaks. The bias may be understood as a consequence of the interference of the waves that perturb the initial density field. Similarly, walls would form between aligned filaments, but it is unclear whether filaments are preferentially aligned. It follows naturally, as suggested by Bond et al. (1996), that X-ray emission from filaments, if there is any, will be more common between clusters that are aligned than otherwise.

Filaments are the source of the material presently infalling to the cluster (see Colberg et al. 1999, for example). Consequently, the clusters determine the location of the filaments that, in turn, determine the accretion mechanism of the clusters. Galactic evolution may be affected by this feedback mechanism, and, indeed, galaxies have been shown to be aligned with the principal axis of the galaxy collection in both clusters (Lambas et al. 1988) and galaxy groups (Fuller et al. 1999). The groups were also found to be preferentially aligned with the nearest Abell clusters.

The new X-ray observatories should be able to either observe filaments or put further constraints on their abundance and luminosity. In particular, the large effective area of *XMM-Newton* (>2000 cm^2 for 1–2 keV compared to 500 cm^2 combined for the *ASCA* Gas Imaging Spectrometer [GIS]) coupled with its wide field of view (30′) allows for the detection of fainter signals than previously possible. Pierre et al. (2000) used numerical simulations to determine if *XMM-Newton* will be able to observe filaments. They give a "good chance" to observe "strong" filaments around $z = 0.1$ but note that the chances decrease as z increases. The primary difficulties that will be encountered are the large size of such objects, as well as selecting a target.

The previously available technology may have been able to detect emission from clusters that were *aligned* along the line of sight. In this case, the accumulated emission boosts the signal so that it is detectable. The environment of the proposed filament, dominated by the galaxy clusters A3391 and A3395, has been reexamined with the view that it may represent a filament alignment. From *ASCA* and *ROSAT* observations of the intercluster region, it is found that there is emission from material spanning the gap between the two clusters, aligned with the axis of the supercluster. We propose that this emission is from filamentary gas.

The paper is laid out as follows. The morphology of the supercluster and description of the components is given in § 2. In § 3.1, the description of the analysis method for the detection of the filament is given, along with the results. We conclude with a discussion in § 4.

All errors are quoted at the 90% confidence level.

2. THE ENVIRONMENT OF THE A3391-A3395 SYSTEM

Galaxy clusters A3391 and A3395 are located in the constellation Carina, SSE1.°5 of the bright star Canopus. The region is about SW26° from the galactic plane and about 10° from the Large Magellanic Cloud. The system has as its members the galaxy clusters 3391, 3395, and S 0584, along with the galaxy group ESO 161-IG 006. Together, they cover a square degree in the sky. A likely member of the system is MS 0620.6−5239, located 1° to the northwest of A3391, adjacent to Canopus. The proximity of Canopus makes optical studies difficult. Consequently, little information exists in the literature on this cluster. A further 4° to the northwest lies Abell 3380. Since it is well separated from the region of interest, its membership is not obvious and it will not be discussed in detail. Both MS 0620.6−5239 and A3380 have a position angle (P.A.) of 35° with respect to A3391.

The galaxy sky surface density was determined for the region surrounding the system (excluding A3380, which is far from the region of interest). The Digitized Sky Survey (DSS) images of a single Second Palomar Observatory Sky Survey (POSS-II) plate of the region[1] were processed by the source extraction tool SExtractor[2] (Bertin & Arnouts 1996). The images were from a single plate. The routine produces a listing of object positions, fluxes, elongations, and FWHMs, among other parameters. The parameters are used to discriminate between galaxies and stars, with galaxies being associated with any object that is particularly dispersed or elongated. A maximum integrated magnitude of 15.5 (minimum integrated signal, 10^5 ADU) was used to limit the selected objects to only the brighter. The threshold for being considered dispersed was a FWHM of more than 5″, while an elongation threshold of the long access being 2 times larger than the short was used. The point-spread function (PSF) for the plate is elongated, presumably owing to tracking errors. The positions of the extracted galaxies were smoothed by an adaptive kernel to produce a number-density field. The adaptive kernel maintained a constant number of 32 galaxies in the density estimate for each point in the field. The field was then smoothed on a scale of 1.′4, equivalent to 200 kpc at the distance of the cluster.

The surface number density for the galaxies is given in Figure 1. No attempt to discriminate against redshift was made. Clusters A3391 and A3395 stand out, along with the galaxy group. MS 0620.6−5239 is partially obscured by Canopus, but is still sufficiently rich to stand above the glare. Upon visual inspection, the four 4 σ peaks south of declination $-54°40'$ were verified to be associated with groups of galaxies. Since no redshifts were available, their association with the system or, for that matter, with each other, is uncertain except for the peak at 6^h25^m, $-55°25'$, which is a galaxy pair at $z = 0.118$ cataloged in the *ROSAT* All-Sky Survey Bright Source Catalog (1RXS). There are no other 4 σ or greater peaks in the field.

[1] http://archive.stsci.edu/cgi-bin/dss_plate_finder.
[2] http://terapix.iap.fr/soft/sextractor/.

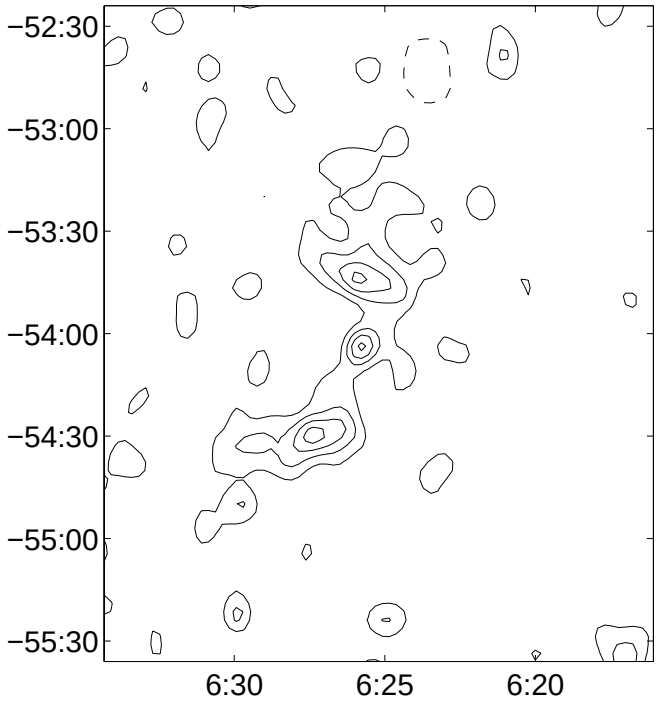

FIG. 1.—The galaxy sky surface density ($m_R < 15.5$) as determined from Digitized Sky Survey-II data using SExtractor to separate galaxies from stars. The contours are at levels of 2, 4, 6, ... σ above the field density. The dashed contour corresponds to the $-2\,\sigma$ level and encircles the bright star Canopus, which masks faint objects.

The redshift distribution among the various structures is illustrated in Figure 2. The galaxy distribution in the vicinity of A3391 and A3395 is given by the contour levels while the color axis gives the mean redshift. To compute the distribution, the 285 galaxies for which radial velocities have been compiled by Teague et al. (1990) were used. Teague et al. selected the original sample by eye, providing an approximately magnitude-limited selection. The errors on the measured radial velocities were typically less than 200 km s^{-1}. We truncated the sample in radial-velocity space to $0.040 > z > 0.065$, removing 73 galaxies. The mean galaxy surface density was determined using an adaptive kernel in the fashion used on the galaxies extracted from the DSS. Similarly, for these galaxies the mean local redshift map was found by averaging redshifts of the nearby galaxies on the sky with an adaptive kernel. In redshift space, AS 0584 (not on the map) is the nearest, at $z = 0.048$. The cluster A3395 has $z = 0.051$, while the galaxy group lies at $z = 0.053$, midway to A3391 at $z = 0.057$. The redshift to MS 0620.6−5239 is not well known, owing to its proximity to Canopus. It is reported to have a redshift of $z = 0.049 \pm 0.002$ (four brightest of five galaxies) (Gioia et al. 1984) and $z = 0.052$ ($V_r = 15300 \pm 300$ km s^{-1}) (Tritton 1972).

Figure 3 shows the X-ray emission of the field as recorded during the *ROSAT* All-Sky Survey. The majority of the X-ray sources are unresolved and included stars such as Canopus, which is the bright object in the northern third of the field. The field is at the southern edge of a swath of diffuse, soft galactic X-ray emission that shows up as an

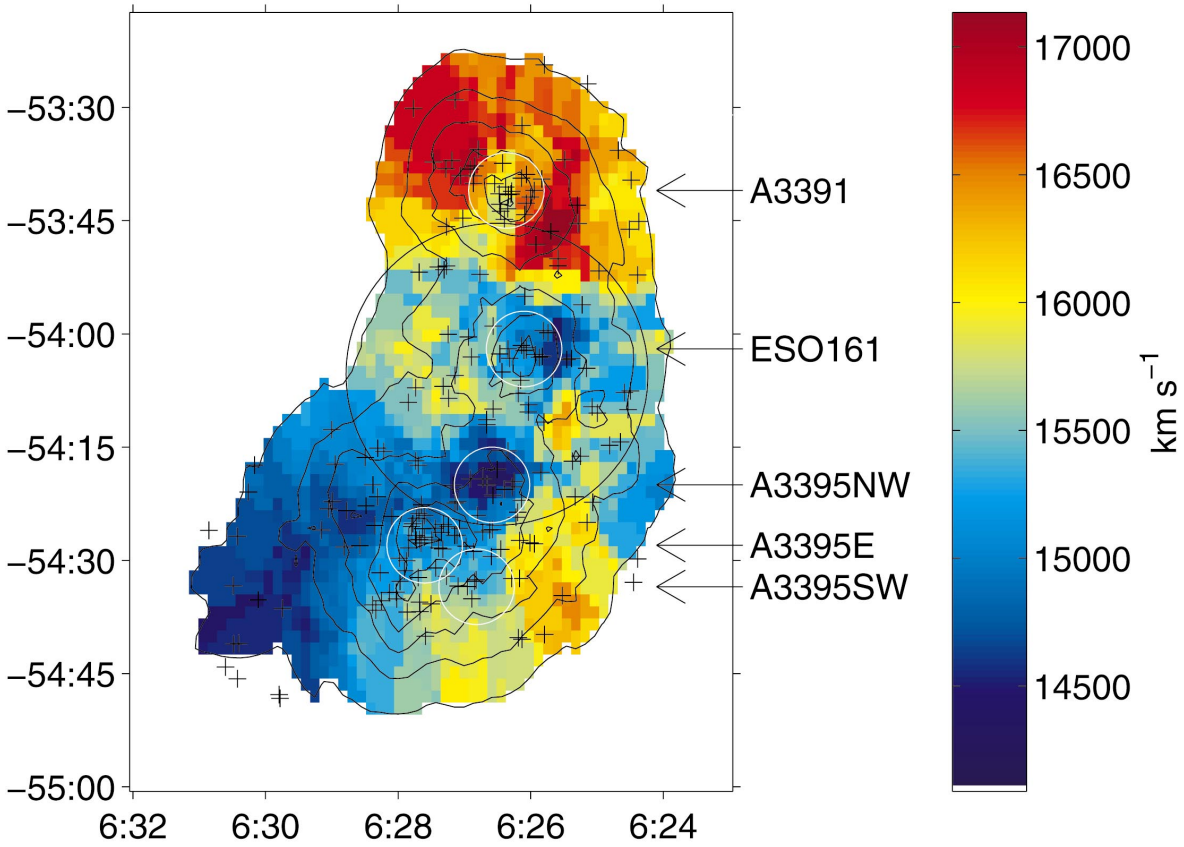

FIG. 2.—The galaxy concentration and mean redshifts. The sample of galaxies is indicated by the crosses. Their mean local density is given by the contour levels, which are separated by factors of 2. The mean local radial velocity is illustrated by the background color scale. Ignore redshift data outside the contours. The position of the white circles correspond to the objects D–H, north to south, listed in Table 1. Their radii are 5′. The larger dark circle is the *ASCA* GIS field of view.

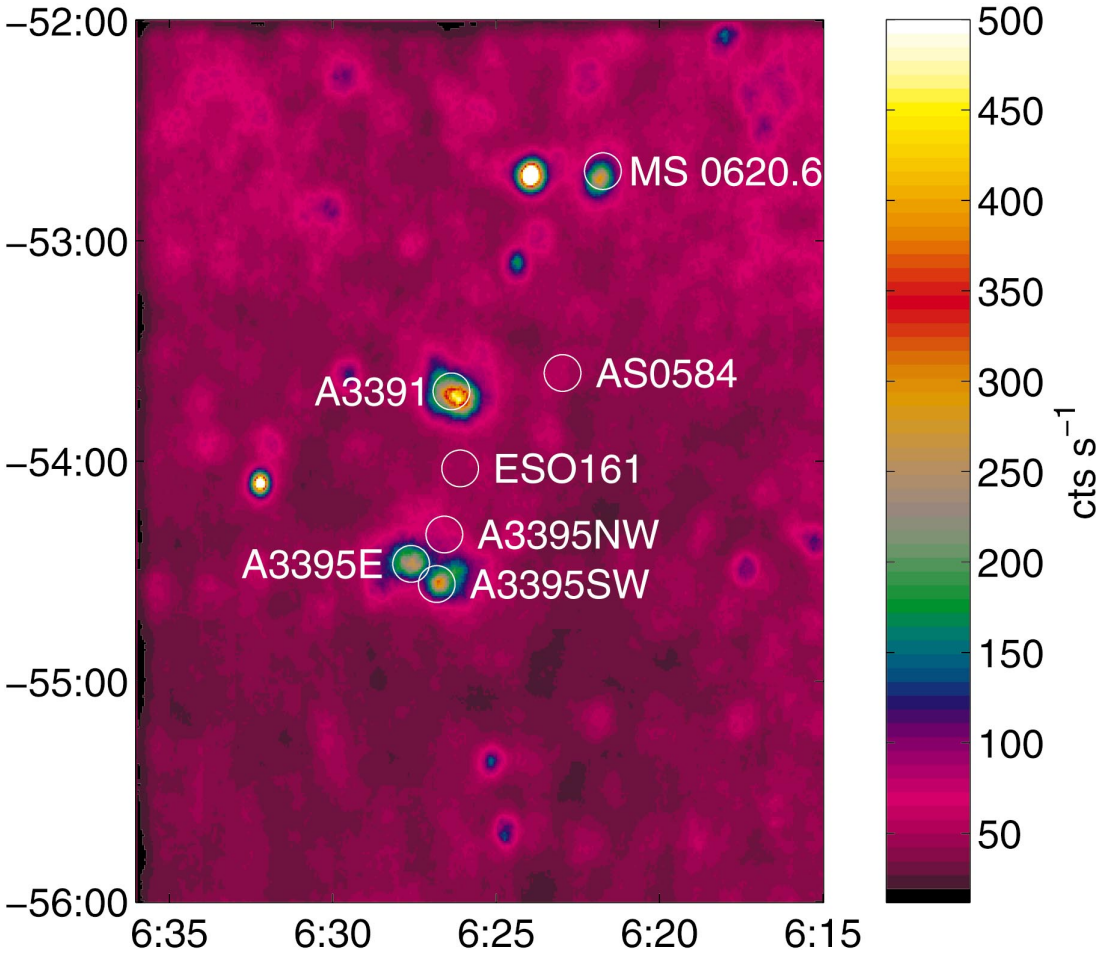

FIG. 3.—The field in the X-ray band from the *ROSAT* All Sky Survey. The positions of the circles correspond to the objects B–H, north to south, listed in Table 1. Their radii are 5′.

increase in the background counts north of the system. Fortunately, the lower edge of the swath terminates north of A3391. The regions circled are the components of the system. Many of the other objects in the field also appear in the galaxy density map, Figure 1, and are discussed above. Every enhancement was cross-referenced with the various catalogs found in the NASA/IPAC Extragalactic Database (NED), but not all were identified. No superposition of a previously cataloged background or foreground object was found.

A3391 is a regular cluster which is dominated by a dumbbell cD galaxy (Teague et al. 1990). It has a luminosity of $(1.6 \pm 0.3) \times 10^{44}$ ergs s^{-1} (0.5–2.0 keV) (De Grandi et al. 1999) and temperature measured from the *ASCA* GIS data to be 6 ± 1 keV (Markevitch 1998). Henriksen & Jones (1996) do not find evidence of a cooling flow using *ROSAT* PSPC data. The mass has been measured to be 2.3×10^{14} h_{65}^{-1} $M_{\odot}$, $r < 1$ Mpc (Henriksen & Jones 1996) using X-ray and optical methods. The dumbbell galaxy is associated spatially with a radio point source with a flux of 1900 ± 200 mJy (Wright & Otrupcek 1990; Wright et al. 1994). The source has a spectral index of $\alpha = -1.1$, which is, given the beamwidth of the 4.2 of the PNM Southern Survey, consistent with radio lobes of an active galaxy. Gregorini et al. (1994) associate the radio source with the eastern lobe of the dumbbell galaxy. Using the VLA, they report resolving it into two components which straddle the lobe in a north-south direction. The separate sources have, from north to south, 6 cm fluxes of 779.9 and 812.5 mJy and upper limits on their angular sizes of 49″ and 31″.

Cluster A3395 is double-peaked in X-ray flux (Henriksen & Jones 1996). Previous works have classified the A3395 system as one potentially undergoing a merging event. Henriksen & Jones (1996) find that the A3395 components have dynamics consistent with infalling, bound objects. They conclude, however, that A3391 is not bound to the A3395 pair. In a study of the temperature and entropy gradients, Markevitch et al. (1998) find little evidence of excess shock heating in the A3395 system, which suggests they are not currently colliding. More recently, Donnelly et al. (2001) have reanalyzed the *ASCA* data correcting for the PSF using the method of Churazov et al. (1996). They find significantly higher gas temperatures between the southwestern and northeastern component of A3395 and conclude that the system is approaching the first core passage.

The galaxy distribution of A3395 is elongated strongly in the northwest-southest (NW-SE) direction, transverse to the axis of the double-peaked X-ray emission. The northeastern component is coincident with the peak of the galaxy distribution while the southwestern is 10′ away. The galaxies in the northeast structure have a lower mean radial velocity, with $V_r = 15{,}000$ km s^{-1}, corresponding to $z = 0.050$, compared with $V_r = 15{,}400$ km s^{-1}, corresponding to $z = 0.051$, for the southwest component. The cluster has a total luminosity of $(1.2 \pm 0.5) \times 10^{44}$ ergs s^{-1} (0.5–2.0

keV) (De Grandi et al. 1999) with the NE component being marginally more luminous [$(5.7^{+2.9}_{-0.4}) \times 10^{43}$ ergs s^{-1} versus $(4.2^{+5.8}_{-0.5}) \times 10^{43}$ ergs s^{-1} (Henriksen & Jones 1996)]. The temperature of the entire structure is reported by Markevitch (1998) to be 5.0 ± 0.5 keV. The strong elongation in the NW-SE direction of the galaxy distribution may be owing to a projection effect. The galaxies clustered 12′ northwest of the center of the galaxy distribution have a distinctly lower redshift ($V_r = 14{,}500$ km s^{-1}, corresponding to $z = 0.048$). There is an increase in the X-ray emission associated with this group of galaxies. Consequently, the cluster may be separated into three components: A3395 E, which coincides with the peak in galaxy concentration and X-ray luminosity; A3395 NW, which coincides with the group of low-redshift galaxies; and A3395 SW, which encompasses the second X-ray emission peak. Masses have been found for the east and southwest components to be $(1.7 \pm 0.5) \times 10^{14}\ h_{65}^{-1}\ M_\odot$ and $(2.9 \pm 0.5) \times 10^{14}\ h_{65}^{-1}\ M_\odot$, $r < 1$ Mpc (Henriksen & Jones 1996). The southwest component is coincident with a radio source with a flux of 1020 ± 80 mJy and $\alpha = -0.9$ (Wright & Otrupcek 1990; Wright et al. 1994), parameters that are again consistent with the radio lobes of an active galactic nucleus (AGN). Gregorini et al. (1994) report a lower flux at 6 cm of 61.7 mJy and associate the source with a giant elliptical in the southwest component. They fail to resolve the source.

The galaxy group ESO 161-1G 006 is visually dominated by a sextet of galaxies in close proximity (<1′). One of the galaxies is an edge-on spiral with a redshift of $z = 0.1468$ that excludes it from the system. Redshifts exist for four of the remaining five, giving a mean recessional velocity for the system of $V_r = 15{,}600$ km s^{-1}, as well as the high velocity dispersion, $\sigma = 1800$ km s^{-1}. The velocity dispersion is too large by a factor of 3–6 to be consistent with a group of galaxies. Indeed, it is double the velocity dispersion of both A3391 and A3395. The system must be either the chance alignment of two pairs of galaxies, a pair and two isolated galaxies, or four isolated galaxies. The western pair of galaxies have radial velocities of 13,600 km s^{-1} and 14,300 km s^{-1} while the eastern pair are receding at 16,800 km s^{-1} and 17,700 km s^{-1}. All the velocity data are from Teague et al. (1990) and have errors on the order of ± 100 km s^{-1}. There is another galaxy 2.′5 to the southwest of the western pair with a redshift of 13,500 km s^{-1}. The X-ray data provide constraints on the nature of the group, as is discussed in § 3.3.

Little information exists for AS 0584. It has a Bautz-Morgan classification of I–II, characterizing the central galaxy between cD and a giant elliptical (Abell et al. 1989). It is curiously lacking an X-ray signature, despite possessing the large elliptical galaxy. The central elliptical has a redshift of $z = 0.047$ ($V_r = 14{,}180$). No redshifts for member galaxies other than the central elliptical have been found in the literature, so this value is adopted for the entire cluster. The center of the elliptical is SSW30″ from a 47 mJy radio source (Wright et al. 1994), but an association with the galaxy has not been established. There is a visible-light object located at the location of the radio source, but no identification for it was found in NED.

The cluster MS 0620.6-5239 is host to the radio galaxy, PKS 0620−526. The reported values for the X-ray flux are 3.316×10^{-12} ergs s^{-1} cm^{-2} measured by *Einstein* (Stocke et al. 1991), a value that accounts for a flux contribution from a nearby star, and $(4 \pm 1) \times 10^{-12}$ ergs s^{-1}cm^{-2} as measured from the *ROSAT* All-Sky Survey data (De Grandi et al. 1999). Using a value of $(4 \pm 2) \times 10^{-12}$ ergs s^{-1} cm^{-2}, this translates into a luminosity of $(3 \pm 1) \times 10^{43}$ ergs s^{-1} (0.5–2.0 keV), making it the fourth most X-ray luminous object of the seven objects in the system (A3395 counting as two objects).

The information regarding the components of the system is summarized in Table 1. It should be noted that at a recessional velocity of 15 000 km s^{-1}, an angular distance of 1° corresponds to 2.6 h^{-1} Mpc while a velocity decrement of 100 km s^{-1} corresponds to 1 h^{-1} Mpc for pure Hubble flow.

2.1. *Filament Geometry*

The distribution of galaxies, four clusters, and a galaxy group in the vicinity of galaxy clusters A3391 and A3395 strongly suggests the alignment of these objects in what could best be described as a filament. The volume and, consequently, the density and total mass of the gas in the filamentary structure is a function of the alignment

TABLE 1

OBJECTS

Object	Name	R.A.	Decl.	X-Ray Luminosity (10^{43} ergs s^{-1})	Temperature (keV)	V_r (km s^{-1})	z
A.....	A3380	6 06 58	−49 29			16700[a]	0.056
B.....	MS 0620.6−5239	6 21 44	−52 41	2.6 ± 1[b]		15300[c]	0.051
C.....	AS 0584	6 22 58	−53 36	< 0.01		14200[d]	0.047
D.....	A3391	6 26 15	−53 41	16 ± 2[e]	4–5[f,g]	16500	0.055
E.....	ESO 161-IG 006	6 26 06	−54 02	0.12 ± 0.01		15600	0.052
F.....	A3395 NW	6 26 35	−54 20	Included in G		14500	0.048
G.....	A3395 E	6 27 37	−54 27	$5.7^{+2.9}_{-0.4}$[f]	$4.1^{+\infty}_{-3.5}$[f]	15000	0.050
H.....	A3395 SW	6 26 49	−54 33	$4.2^{+5.8}_{-0.5}$[f]	$4.6^{+\infty}_{-3.1}$[f]	15400	0.051

NOTE.—Units of right ascension are hours, minutes, and seconds, and units of declination are degrees, arcminutes, and arcseconds.

[a] Abell et al. 1989.
[b] Gioia et al. 1984.
[c] Tritton 1972.
[d] Struble & Rood 1999.
[e] De Grandi et al. 1999.
[f] Henriksen & Jones 1996.
[g] Markevitch 1998.

geometry. The important element of the geometry is the angle between the line of sight and the long axis of the system. Here we will refer to this angle as the *inclination* of the system. The limits on the inclination may be ascertained by spatial and dynamical arguments. Since the region of interest spans the space between A3391 and A3395, we will limit the analysis to the A3391-A3395 pair and the A3395 system itself. Note that the inclinations of the two systems are uncorrelated. We will show that the A3391-A3395 system is unbound, implying that the system is being viewed at a low inclination. As a point of interest, it will also be shown that there exists an unbound solution for the A3395 system, but it is most likely bound.

Fundamental to the argument are the concepts of peculiar velocity, turnaround radius, and bound solutions. These concepts may be understood by considering two overdense regions of the universe, in which the clusters will subsequently form, separated by some initial distance and unperturbed by other masses other than the isotropic mass density of the universe. The regions are initially in motion away from each other, fixed in the Hubble flow. Their mutual gravitational attraction will slow the rate of separation. That is, each region will break from the Hubble flow and they will each develop a *peculiar velocity* in the direction of the other region. If the regions have sufficient mass, the gravitational attraction will overcome the initial kinetic energy and they will slow to a stop (at which point their peculiar velocities are equal and opposite to their Hubble flow velocities). It is at this point that the regions have reached *turnaround radius.* Barring any further input of energy from outside sources, the regions will fall toward each other. In this case, the regions will be *bound*, since their dynamics will never take them further away from each other than the turnaround radius. A *bound solution* is a set of velocities for the regions and a separation between them such that the system is bound. If the system is unbound, turnaround is never achieved.

For a system to be unbound, the total internal kinetic energy must be greater than the total gravitational potential energy. For a pair of clusters, A and B, the inequality that tests if the system is unbound is

$$\frac{1}{2}\left(M_A v_A^2 + M_B v_B^2\right) > G\frac{M_A M_B}{R}, \tag{1}$$

where M is the mass of a cluster, v is the velocity of a cluster relative to the center of mass of the system, and R is the separation between the two clusters. For unbound systems, the velocity component along the axis of separation dominates the magnitude of the velocity. Any nonaxial motions will only increase the kinetic energy of the system, making it more likely to be unbound. Hence, to simplify the analysis, all velocities are assumed to be along the axis of separation. What is observed is the difference in the radial velocities of the clusters, ΔV_r, and their angular separation on the sky. The angular separation on the sky may be translated into a tangential separation, R_T, using Hubble's law and the observed redshifts. The true separation relates to the tangential separation by $R = R_T/\sin i$, with i the inclination between the line of sight and the axis of the system. The masses of the clusters can be estimated from X-ray analysis of the hot halos or dynamical studies of the constituent galaxies, both of which are done in Henriksen & Jones (1996) for the A3391-A3395 system (see § 2). The velocities, v_A and v_B, are related to their radial components by $v = v_r/\cos i$. Finally, we need the relations to derive the radial components of the velocity of the clusters with respect to the center of mass. The relations are

$$v_{r,A} = \frac{\Delta V_r M_B}{M_A + M_B}, \quad v_{r,B} = -\frac{\Delta V_r M_A}{M_A + M_B}. \tag{2}$$

Combining equation (1) with equation (2) and the relations of R to R_T and v to v_r gives the inequality

$$\frac{1}{2}\frac{R_T \Delta V_r^2}{M_A + M_B} > \cos^2 i \sin i, \tag{3}$$

which is the inequality that may be used to determine unboundedness.

Use of equation (3) with the parameters for the A3391-A3395 system demonstrates the system is unbound. For this system we have the following parameters. The tangential separation is $R_T = 3.1 \pm 0.2\ h_{65}^{-1}$ Mpc with the errors estimated by comparing angular separations of peaks in the X-ray emission and in the galaxy density. The velocity difference is given by $\Delta V_r = (16{,}750 \pm 200) - (15{,}100 \pm 200)$ km s^{-1} $= 1650 \pm 300$ km s^{-1} (errors 1.6 σ) determined from 62 galaxies for A3395 and 26 galaxies for A3391. The radial velocities were taken from the sample of Teague et al. (1990). Finally, the masses, as determined in Henriksen & Jones (1996), are $M_{\rm A3391} = (2.3 \pm 0.5) \times 10^{14}\ h_{65}^{-1}\ M_\odot$ and $M_{\rm A3395} = (2.9 \pm 0.5 + 1.7 \pm 0.5) \times 10^{14}\ h_{65}^{-1}\ M_\odot$. The left-hand side of the inequality, equation (3), is then $1.4 \pm 0.5\ h_{65}^{-1}$. The maximum value possible for $\cos^2 i \sin i$ is 0.38. The system is unbound by at least a factor of 2.4 (90% confidence), which agrees with Henriksen & Jones, who find no bound solutions unless the total mass of the system is 3–4 times larger.

The test, equation (3), may also be used on the two principal components of A3395: A3395E and A3395SW. For the east and southwest components we have $R_T = 0.68 \pm 0.05\ h_{65}^{-1}$ Mpc, $\Delta V_r = (15{,}700 \pm 300) - (15{,}100 \pm 300)$ km s^{-1} $= 600 \pm 400$ km s^{-1}, $M_{\rm A3395SW} = (2.9 \pm 0.5) \times 10^{14}\ h_{65}^{-1}\ M_\odot$, and $M_{\rm A3395E} = (1.7 \pm 0.5) \times 10^{14}\ h_{65}^{-1}\ M_\odot$. In this case, the left-hand side of the inequality is then 0.06 ± 0.07. The maximum range of inclinations for which the inequality is true spans 0°–8° and 68°–90°.

A constraint on the inclination is provided by comparing the speed with which the clusters are moving away from each other to the total distance separating them. Two assumptions are required. First, to simplify the analysis it will be assumed that all cluster motions are directed away from each other. If the clusters are unbound, then the Hubble flow dominates motions which justifies the assumption. Second, it is taken that the velocity of separation in the past was never less than the present velocity of separation. These assumptions lead to the condition that the distance separating the clusters must be greater than the distance by which the clusters could be separated if they moved at the same speed as they do at the present for the duration of the Hubble expansion, i.e., $R > Vt$. This inequality, expressed in terms of measurable velocities and separations as well as the inclination and the age of the system at the given redshift is

$$\frac{R_T}{\Delta V_r\, t(z)} > \tan i. \tag{4}$$

For $z = 0.053 \pm 0.002$ (error covers range in redshift space of A3391 and A3395), $t(z) = 13.75 \pm 0.05\, h_{65}^{-1}$ Gyr for $\Omega_\Lambda = 0.7$ and $\Omega_m = 0.3$ (see eq. [3.63] of Peacock 1999). For the A3391-A3395 pair, the left-hand side of the inequality is 0.13 ± 0.03, which implies a valid range for i of 0°–9°. Similarly for the A3395 system, the only valid range in inclination is 0°–7°.4. Hence the A3391-A3395 system is further constrained by this analysis. For the A3395 E-A3395 SW system, the range of inclinations 68°–90° is excluded, which lowers the probability that the system is unbound to less than 10%, but does not exclude it.

A final constraint provides a minimum value for the inclination, i. The constraint is provided by the maximum possible true separation that is consistent with the measured velocity difference and the Hubble flow. Since $R = R_T/\sin i$ and we observe the tangential separation, R_T, if the inclination, i, goes to zero, the inferred true separation, R, of the clusters would have to go to infinity. There is a limit to how large R can actually be, which puts a lower limit on i. As R goes to large distances, the cluster dynamics become dominated by the Hubble flow. That is, $V \rightarrow HR$. The deviation of the velocity from the true Hubble flow is the peculiar velocity, V_p, such that $V = HR - V_p$. The maximum separation possible is then $[V + \max(V_p)]/H$. The maximum peculiar velocity is estimated by finding the kinetic energy converted to gravitational energy as the clusters separate from an initial separation to a maximum possible separation (infinity). The initial separation is taken to be 1 Mpc. In the standard cosmology, the masses were once arbitrarily close. The perturbations required to generate peculiar velocities, however, did not occur until structure was developed at a redshift of ~ 10. Since we already have a maximum possible inclination for the A3391-A3395 system of $i < 9°$, then the true separation is at least $3.1 \pm 0.2\, h_{65}^{-1}$ Mpc/sin $i = 20 \pm 1\, h_{65}^{-1}$ Mpc. Scaled down by an expansion factor of 10 (a redshift of 11) gives 2 Mpc for an initial separation, which is twice our presumed value. Using 1 Mpc as the initial separation, the maximum peculiar velocity is 1400 km s^{-1}. The maximum true separation is then $(1650 \pm 300 \text{ km s}^{-1} + 1400 \text{ km s}^{-1})/H_0 = 47 \pm 9\, h_{65}^{-1}$ Mpc. This separation implies the minimum inclination is 3°.1.

The constraints outlined above confine the inclination of the A3391-A3395 system to the range 3°.1–9°. Equivalently, the inclinations correspond to a range of ratios of 1:6 to 1:18 for the depth versus the transverse separation. The filament is being observed nearly lengthwise. For the A3395 system itself, the existence of an unbound solution is found. The geometry required for the unbound solution is consistent with the geometry found for the A3391-A3395 system as a whole. The solution is not valid, however, if the structures are presently interacting, as indicated by the presence of hot gas between the lobes.

3. ANALYSIS

3.1. *Data*

In the HEASARC X-ray data archives[3] there are *ROSAT* and *ASCA* observations of the A3391, A3395, and the intercluster region. The data for the intercluster region are provided by the *ASCA* GIS and Solid-State Imaging Spectrometer (SIS) instruments. Only those SIS data taken at a high bit rate were used. From *ROSAT*, data exist for only the two clusters. The *ROSAT* PSPC instrument, however, has a substantially larger field of view than either of the *ASCA* detectors, so the PSPC observations cover the region between the clusters. A summary of the observations used in this study is made in Table 2. In addition to the target observations listed in Table 2, the *ROSAT* All-Sky Survey data retrieved from Max-Planck-Institut für extraterrestrische Physik[4] were also used for testing for scattered light in the *ASCA* observations.

3.2. *Filament*

3.2.1. *ASCA GIS*

As a preliminary analysis, the GIS event file was used to produce an image of the region between A3391 and A3395. The 26603 events from both GIS detectors were smoothed with an adaptive kernel that maintained 100 events within its smoothing radius. The kernel used is a spline with a general Gaussian shape but compact (goes to 0 in a finite distance). The smoothing produced an image with a signal to noise ratio (S/N) of approximately 10. The image was then smoothed with a Gaussian with a full width at half-maximum of 2′. The procedure produces an image with a minimum S/N level throughout the image plane and a resolution no better than that allowed by the GIS instrument.

The background was estimated using the FTOOLS[5] utility, *mkgisbg*, and the blank sky events database.[6] The background events were smoothed using kernels with the same radii as used to smooth the GIS events, followed by convolution with a 2′ FWHM Gaussian. An exposure map

[3] http://heasarc.gsfc.nasa.gov/docs/corp/data.html.
[4] http://www.xray.mpe.mpg.de/cgi-bin/rosat/rosat-survey.
[5] http://heasarc.gsfc.nasa.gov/docs/software/ftools/ftools_menu.html.
[6] ftp://legacy.gsfc.nasa.gov/caldb/data/asca/gis/bcf/bgd/no_sources/.

TABLE 2

OBSERVATIONS

Date	Archive No.	Instrument	Data Mode[a]	Counts	Live Time (s)
1997 Dec 13	85043000	*ASCA* GIS 2		12411	24167
		ASCA GIS 3		13594	24167
		ASCA SIS0	Bright	1596	6747
			Bright2	2091	6747
		ASCA SIS1	Bright	505	3335
			Bright2	812	3335
1992 Apr 3.....	rp800080n00	*ROSAT* PSPC			6461
1991 Mar 24.....	rp800079n00	*ROSAT* PSPC			2595

[a] SIS only.

was created using the FTOOLS utility, *ascaeffmap*, so that the image may be corrected for vignetting. The exposure map was also smoothed in the same fashion as the background events. Consequently, for each position in the image plane, the events, background, and exposure map are smoothed over equal regions of influence. The background was subtracted from the events image and the result was divided by the exposure map.

The *ASCA* GIS image is given in Figure 4. There is a clear enhancement in X-ray emission in the region between the cluster A3395 to the south and the galaxy group located near ($6^h26^m0^s$, $-53°0'$), following a north-northwesterly trend.

Better statistics were achieved by examining the total signal in the region of the lineament. A mask for the GIS data which included the filament region but excluded those areas within 15′ of A3391 and A3395 as well as within 3′ of the galaxy group was created. The included area covered 311 arcmin^2. The count rates within this region were extracted from the data. The count rate contributed by the background was again estimated using the blank sky events database, but for just the region of interest. Data were extracted from energy channels 68–849 (0.8–10 keV, nominally).

The count rate above that expected for the background in this region was found to be $(5.8 \pm 0.3) \times 10^{-2}$ counts s^{-1} and $(6.5 \pm 0.3) \times 10^{-2}$ counts s^{-1} for the GIS2 and GIS3 detectors, which differ marginally in their gain. Using the routine PIMMS, these count rates were translated into fluxes, assuming a Raymond-Smith model (Raymond & Smith 1977) with the hydrogen column density set to $n_H = 5.6 \times 10^{20}$ cm^{-2}(Dickey & Lockman 1990). Since the detector is most sensitive to gas at a temperature of 1.3 keV, the flux estimate from a model with this temperature would represent a lower limit to the true flux. If the temperature of the gas is estimated to be either 0.5 or 2 keV, then the estimated flux rises to 25×10^{-13} ergs cm^{-2} s^{-1} and 18×10^{-13} ergs cm^{-2} s^{-1}, respectively. Consequently, lower limits of 13×10^{-13} ergs cm^{-2} s^{-1} and 15×10^{-13}ergs cm^{-2} s^{-1} (0.8–10 keV) for the GIS2 and GIS3 were found presuming $T = 1.3$ keV. Here and elsewhere in the paper, lower limits are 3 σ below the measured value. The flux rises sharply as the input gas temperature drops, which is significant since it would be expected that filament gas would be less than 1 keV.

The flux-to-luminosity relation for a $z = 0.5$ object, $L = 6.4 \times 10^{54}\ h_{65}^{-2}$ cm^2 F, gives a lower limit to the luminosity of $8 \times 10^{42}\ h_{65}^{-2}$ ergs s^{-1} in the 0.8–10.0 keV energy band. The luminosity is approximately 1/10 the luminosity of A3395 (Henriksen & Jones 1996) and 1/15 of A3391.

The sample area corresponds to approximately 1.4 h_{65}^{-2} Mpc^2 (305 arcmin^2), giving an approximate lower limit to the surface luminosity of $\mathscr{L} \simeq 6 \times 10^{42}$ ergs s^{-1} Mpc^2 and a surface brightness of $2.6 \times 10^{40}\ h_{65}^{-2}$ ergs s^{-1} arcmin^{-2}.

3.2.2. *GIS Scattered Light*

The count-rate in the field of the *ASCA* GIS detector for the intercluster observation is contaminated by stray photons from the comparatively bright sources A3391 and the components of A3395. There are three independent causes of light scattering (Tsusaka et al. 1995): (1) nonideal optical paths, (2) broadening owing to reflector misalign-

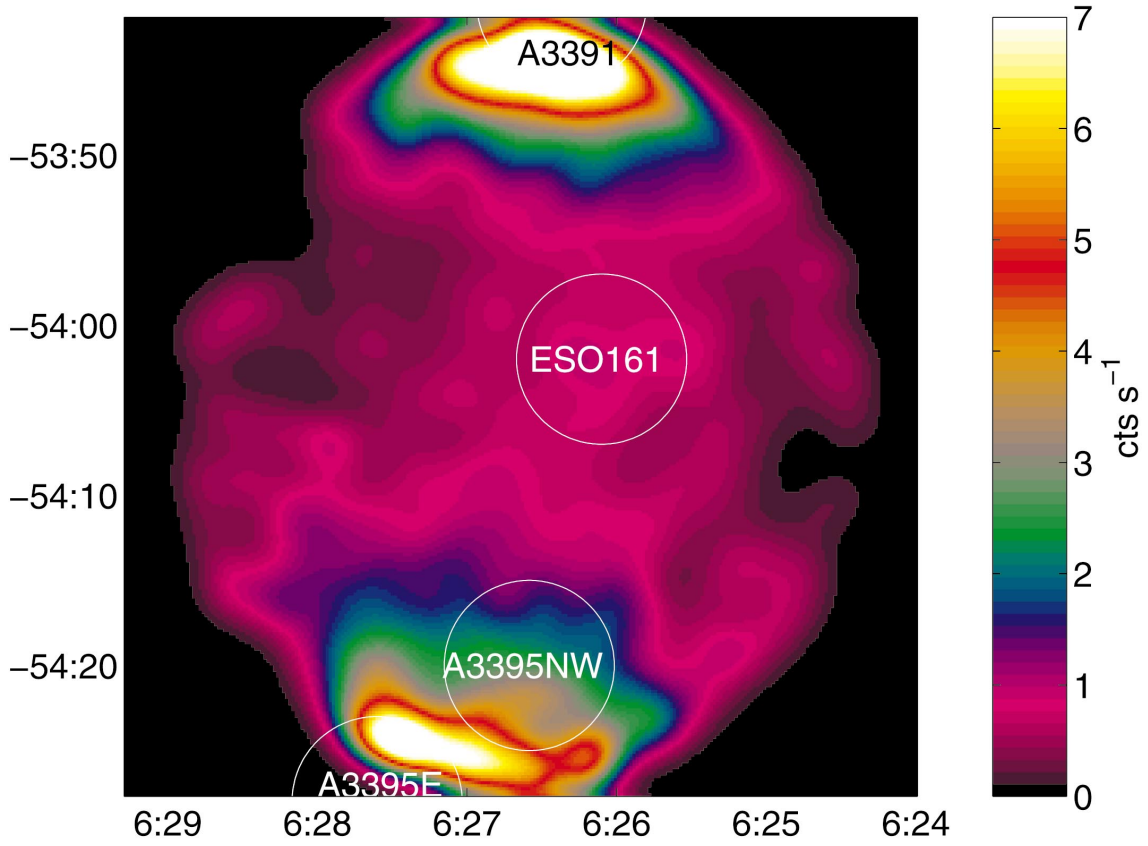

FIG. 4.—The GIS image of the region between A3391 and A3395. The image has had the background rate subtracted. The count rate is events per second per detector. The circles have radii of 5′ and are centered on A3391, the galaxy group, A3395 NW, and A3395 E, respectively, from north to south.

ment and surface distortion, and (3) diffraction by surface roughness. Nonideal paths are those other than the primary optical path, and involve grazing reflections off of the front surface of both the primary and secondary mirrors. The nonideal paths are limited to direct passage without reflection, reflection only by the primary mirror, reflection only by the secondary mirror, and multiple reflections off of the backs and fronts of the mirrors. Since the angle to which grazing maintains its efficiency for reflection off of both the front and back sides is energy dependent, the scattering contributed by nonideal paths decreases with increasing energy. Surface fluctuations and misalignment cause geometric scattering, which is energy independent. Finally, scattering via diffraction increases with photon energy. A method must be used to account for this contamination. Ray-tracing provides the means to determine the proportion of photons scattering into the region of interest.

We used two ray-tracing methods to create scattered light maps of the region between the clusters. The first uses model sources as input while the other is able to use a flux map of the region covering the observation field of view as input. The FTOOLS package, *ascaray*, performs ray-tracing using predefined model sources as input. For ray-tracing from an input flux map, the *ASCA* analysis tool, *trace_asca* (Ptak 1997; Ptak et al. 1997) was used.

Both *ascaray* and *trace_asca* are able to model sources outside the field of view. They have, at their core, the same legacy routines developed for preflight characterization of the *ASCA* XRT. Those routines were able to reproduce the scattered light to better than 10% for a source 1° off-axis (Tsusaka et al. 1995). In-flight validation of the ray-tracing software has been sparse. The ray-tracing code has been tested to up to 100′ off-axis using observations of the QSO 3C 273, with the stray light flux being modeled[7] to better than 20% within 1° and a factor of 2 within 1.′40. Ptak (1997) finds good agreement in reproducing the image of 3C 273 by *trace_asca* but tests only up to 10′ off-axis. The principal sources of stray light in this GIS image of the intercluster region are A3391 and the components of A3395 that are located 30′ from the center of the field of view.

3.2.2.1. *Ray-Tracing with ascaray*

In the following results, the scattered light contributions from A3391 and the components of A3395 were determined independently by modeling each using the FTOOLS package, *ascaray*. Four objects were modeled, A3395 E, SW, and NW, and A3391. The objects were presumed to have flux distributions consistent with β-models, the parameters for which were taken from Henriksen & Jones (1996). The parameters for A3395 NW, however, were determined separately by first performing this analysis on the *ASCA* GIS observation of A3395 and selecting a set of parameters (β and core radius) which best reproduced the observed distribution. The core radii were 1.′1, 1.′5, 2.′5, and 1.′5 for A3395 E, SW, and NW, and A3391, respectively. The routine, *ascaray*, is not able to accept values for β that are less than 0.51 (otherwise an internal integral diverges) and Henriksen & Jones (1996) assign values to β of 0.33, 0.47, and 0.49, to A3395 E, A3395 SW, and A3391, respectively. Consequently, the minimum value of $\beta = 0.51$ was used for all models. This limitation is a point of concern and will be discussed below.

[7] http://heasarc.gsfc.nasa.gov/docs/asca/dec95/min5.html.

For each component, the scattering of 1,000,000 photons in each of the energies, 0.6, 0.8, 1.0, 1.5, 2.0, 3.0, 4.0, 5.0, and 7.0 keV, was simulated using *ascaray*. The 12 different simulations were co-added to produce a single image of the scattered photon distribution. The contributions from the different energy bands were weighted by the factors 0.06, 0.11, 0.20, 0.26, 0.18, 0.08, 0.05, 0.03, and 0.02, respectively. The factors were derived from the photon energy data from the *ASCA* GIS observations of A3391 and A3395. The contributions from each component were also weighted by their relative luminosities as measured from *ASCA* observations.

It was found that photons in the 0.6–1.0 keV range were twice as likely to be scattered as photons in the 4.0–7.0 range. Thus the spectrum of the scattered light will be softer than the cluster spectra.

The photon distribution from the simulations of the stray light is shown by Figure 5. The routine fails to recreate the shapes of the peaks associated with the edges of the clusters A3391 and A3395 as observed by the GIS (Fig. 4). The inability to successfully model the flux distribution may be caused by the use of values for β that are larger than appropriate. The core radii in the input to *ascaray* were subsequently varied in an attempt to compensate for the larger values of β used as input, but no combination was found to produce satisfactory results. The failure diminishes the confidence we have in the results from using this tool. Nevertheless, we note that approximately 0.5% of the photons from the cluster components are scattered into the intercluster region associated with the filament. The contribution corresponds to a flux of approximately 2×10^{-13} ergs s^{-1} cm^{-2}, or about 1/7 of the lower limit provided by the GIS data. A second ray-tracing method, however, is required to verify this result.

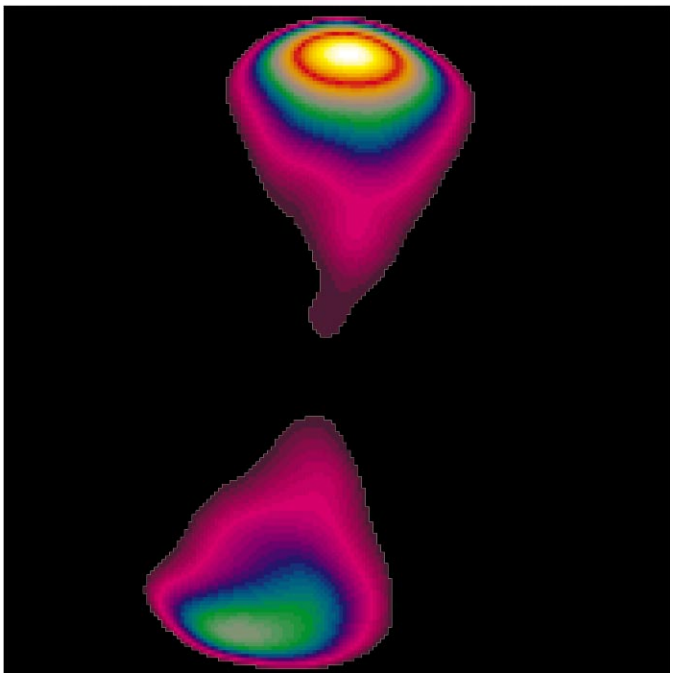

FIG. 5.—The distribution of light scattered onto the image plane of the GIS detector from A3391 and the components of A3395. The distribution was determined using the FTOOLS package *ascaray*. See the text for more details.

3.2.2.2. *Ray-Tracing with trace_asca*

A different approach is provided by the *ASCA* analysis tool, *trace_asca*[8] (Ptak 1997). The tool is able to take a flux map as input and, as such, is able to trace photons coming from the sources within and surrounding the field of view. For a template, the *ROSAT* All-Sky Survey data were used to create an X-ray intensity map of the sky in the region, 2° square, surrounding the center of the GIS field of view. The emission, weighted by the X-ray intensity map, was presumed to be from a 5 keV gas emitting via thermal bremsstrahlung radiation. These parameters were selected since the bulk of the emission is coming from the clusters A3391 and A3395.

Two input images were created from the *ROSAT* All-Sky Survey data: one unmodified and one with the intercluster emission "blanked" (Fig. 6, panels *a* and *b*), since filamentary emission is weakly visible in the PSPC image. For the blanked image, a rectangular region between A3391 and A3395 was set to a constant count-rate approximate to that in the field away from the clusters. If a significant count-rate is predicted in the intercluster region using the blanked image as input, it may be taken as indicative of a strong contribution from scattered light.

The ray-traced flux rates calculated from the input images are given in Figure 6, panels *c* and *d*. The excess emission north of A3395 seen in panel *c* is entirely absent in panel *d*, confirming that the counts are from flux originating in the intercluster region and not from photons scattered into the field from A3391 or A3395. That the shapes of the bright peaks at the northern and southern edges are similar to those observed in the GIS image (Fig. 4) indicates that the routine is faithfully modeling the scattering.

An input map with the blanked region set to zero was ray-traced to determine the contribution scattered photons make to the filament region. For the ray-traced image using the unaltered input map, less than 7% of the counts in the filament region come from outside the blanked region. The

[8] http://lheawww.gsfc.nasa.gov/~ptak/trace2/.

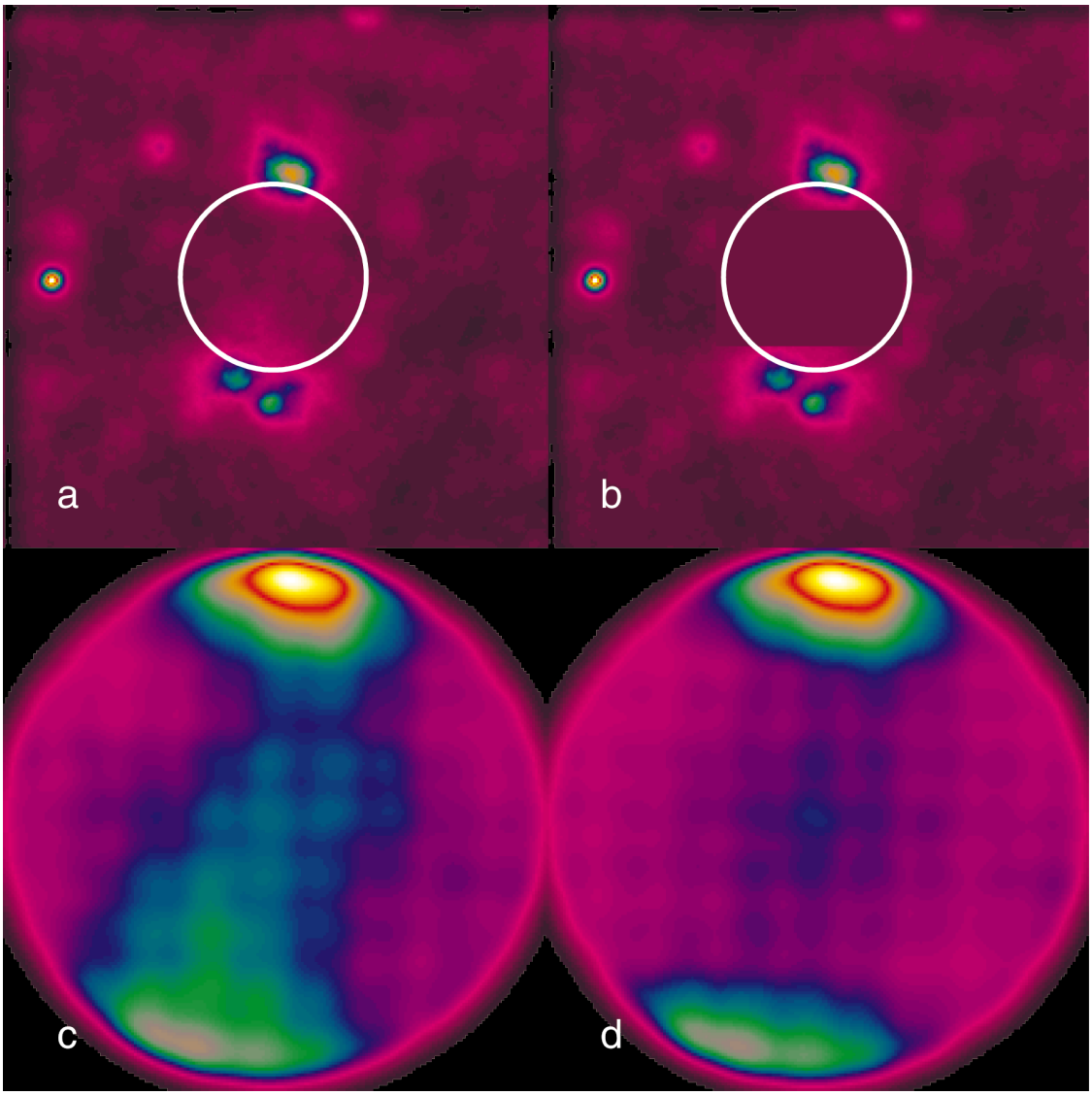

FIG. 6.—The distribution of light, including scatter, estimated to be measured at the image plane of the GIS detector by image ray-tracing. As input, *ROSAT* All-Sky Survey data (*top row*) were used. The ray-tracing was done by the tool *trace_asca*. Image *a* was traced to produce image *c*. Image *b* had the intercluster field "blanked," which was subsequently ray-traced to produce image *d*.

fraction is almost $\frac{1}{2}$ of the 13% calculated using *ascaray*. To err on the side of caution, we will still correct the *ASCA*-measured fluxes by 13%, as is done in Table 3.

3.2.3. *ASCA SIS*

The data recorded by the SIS cameras on *ASCA* were used to determine if a flux from the filament was detected. The field of view of the SIS cameras is small (a square with sides spanning 22′). The field of view of the SIS camera was centered on ($6^h26^m35^s$, $-54°3'32''$), which is 5′ from the galaxy group. No attempt to remove any signal that originates from the galaxy group was made.

A mask was generated that selected the active regions of the four SIS chips. The events in these regions were limited to those that had energies between 0.5 and 6 keV (PI channels 136–1333 in BRIGHT mode and 137–1644 in BRIGHT2 mode). Outside this range, the effective area of the cameras drops off considerably.

Background rates were also determined for the selected region within the given energy range using archived background files.[9]

The count rates above the background for the entire SIS field were found to be $(6.6 \pm 0.5) \times 10^{-2}$ and $(5.0 \pm 0.8) \times 10^{-2}$ counts s^{-1} for the SIS0 and SIS1 cameras, respectively. The rates were converted to fluxes using PIMMS, assuming the same Raymond-Smith model used earlier. Since the SIS is more sensitive to cooler photons, to get a lower limit on the flux an input temperature of 0.3 keV was used. The lower limits to the flux were found to be 1.3×10^{-12} ergs cm^2 s^{-1} and 1.0×10^{-12} ergs cm^2 s^{-1} for the 0.5–6 keV energy band. Again, the errors arising from the assumptions of the model are larger than the quoted errors. A lower limit, $F \gtrsim 10 \times 10^{-13}$ ergs cm^2 s^{-1}, is inferred. The minimum flux corresponds to a luminosity of $6 \times 10^{42}\ h_{65}^{-2}$ ergs s^{-1}.

3.2.4. *ROSAT PSPC*

Data from *ROSAT* PSPC pointed observations of A3391 and A3395 were taken from the archives (Table 2).

It is unfortunate that the region of the filament is partially obscured behind a radial rib for the A3395 observation. There is some emission visible to the right of the rib in the vicinity of the galaxy group. In the case of the A3391 data, the galaxy group is obscured behind the circular rib circumscribing the principal field of view. The filament region is visible, however, permitting better statistics in the search for emission in the filament region compared with the A3395 data.

To get count rates and lower limits to the flux, the *ROSAT* PSPC events data were processed in the following manner. The region used to extract the filament from the *ASCA* GIS data was converted to PSPC image coordinates. The counts within this region which fell in the PI channels 40–200 (0.4–2.0 keV) were extracted. The count rate was determined by dividing the counts (per binned pixel, at this point) by the vignetting-corrected exposure map. The exposure map was created using the detector map for the PI channels of 42–201, which most closely spans the energy range considered here. The background was estimated by selecting counts in 10 regions away from the filament, clusters, and obvious point sources. The background count rate was also normalized by the same exposure map. The background count rate was then scaled by the ratio of the area of the filament region and the background region. The event rate for the filament is then estimated to be the event rate within the region less the scaled background rate. The processing was done for the *ROSAT* PSPC data for A3391 and A3395. Count rates of $(6.8 \pm 0.5) \times 10^{-2}$ counts s^{-1} and $(6.4 \pm 0.3) \times 10^{-2}$ counts s^{-1}, respectively, were found. The rates are translated by PIMMS to minimum fluxes of 5.2×10^{-13} ergs s^{-1} cm^{-2} and 4.7×10^{-13} ergs s^{-1} cm^{-2}, presuming a temperature of 0.6 K. This temperature minimizes the calculated flux. Hence, the fluxes represent lower limits. The corresponding minimum luminosity is then $3.0 \times 10^{42}\ h_{65}^{-2}$ ergs s^{-1}.

3.3. *Galaxy Group*

Emission from the galaxy group is evident in the *ASCA* GIS data illustrated in Figure 4. A flux estimate was made for the galaxy group using an analysis similar to that used for the filament region in § 3.2.1. A circular aperture 3′ in radius was used to isolate the group. The count rate within this region was found, as was the background rate from the source-free regions.

The total number of counts is 5 σ above the background. When converted to a flux using PIMMS, assuming $T = 1$ keV, a value of $(2.0 \pm 0.3) \times 10^{-13}$ ergs cm^{-2} s^{-1} (0.8–10 keV) is found for both the GIS2 and GIS3 data. The corresponding luminosity is then $(1.2 \pm 0.2) \times 10^{42}\ h_{65}^{-2}$ ergs s^{-1}. The luminosity is about $\frac{1}{8}$ of the total flux from the fila-

[9] ftp://legacy.gsfc.nasa.gov/caldb/data/asca/sis/bcf/bgd/.

TABLE 3

MEASURED FLUX LOWER LIMITS

INSTRUMENT	ENERGY WINDOW (keV)	F (10^{-13} ergs s^{-1} cm^{-2})	
		Lower Limit	$T = 1$ keV, 0.4–10 keV[a]
ASCA GIS 2	0.8–9.0	$\gtrsim 12.9 \pm 0.8$[b]	20 ± 1
ASCA GIS 3	0.8–9.0	$\gtrsim 14.6 \pm 0.8$[b]	22 ± 1
ASCA SIS 0	0.5–6.0	$\gtrsim 10.1 \pm 0.6$[b]	11.7 ± 0.8
ASCA SIS 1	0.5–6.0	$\gtrsim 7.7 \pm 0.6$[b]	8.9 ± 0.8
ROSAT PSPC (A3391).....	0.4–2.4	$\gtrsim 6.2 \pm 0.5$	6.8 ± 0.5
ROSAT PSPC (A3395).....	0.4–2.4	$\gtrsim 5.8 \pm 0.6$	6.4 ± 0.8

[a] $n_H = 5.6 \times 10^{20}$ cm^{-2}.
[b] Corrected for a 13% contribution from scattered light.

ment, but since the projected area is 9 times smaller than the filament's, the surface flux is slightly greater.

We were unable to use either the SIS or PSPC data to determine the galaxy group luminosity. The group was not completely in the field of view of the SIS camera, and was unfortunately masked either partially or completely by the support ribs of the PSPC instrument in the observations of A3391 and A3395.

3.4. *AS 0584*

The region of AS 0584 was observed serendipitously by *ROSAT* in its observation of A3391. Approximately half of the region of interest was partially obscured by a rib support. The telescope jitter was transverse to the rib, however, leading to an attenuation of the signal not exceeding 20%, a value determined by examination of the exposure map. A similar analysis was performed as for the filament region to put an upper limit on the flux from the cluster AS 0584. A circular aperture with a 4′ radius centered on the cluster was used to extract the recorded events from the PSPC data. After background subtraction, a count rate of $(1 \pm 2) \times 10^{-3}$ counts s^{-1} was determined. The rate obviously represents a null detection. The 3 σ count rate corresponds to a flux of 4.5×10^{-14} ergs cm^{-2} s^{-1}, giving an upper limit to the luminosity of 3×10^{41} h_{65}^{-2} ergs s^{-1}.

There is no appreciable enhancement in the galaxy density in the location of AS 0584 (Fig. 1). There is a bright elliptical at the location of the cluster that is classified as a cD galaxy by Abell et al. (1989). However, examination of the region using second generation Deep Sky Survey images[10] processed with SExtractor using the same criteria as described in § 2 finds no concentration of galaxies above the background. Altering the criteria failed to reveal a faint population. This is confusing, since Abell clusters are identified by a local enhancement in galaxy density (specifically, at least 30 galaxies with magnitudes between the magnitude of the third brightest member and that plus two). We are unable to explain this apparent misidentification.

The limit on the X-ray flux from the elliptical further points to the absence of a cluster at the given location. From a sample of X-ray–selected clusters containing cD galaxies examined by Burns (1990), a span in X-ray luminosity for the clusters was found to be 3×10^{43} ergs s^{-1} to 2×10^{45} ergs s^{-1}, fully 2 orders of magnitude greater than the found for the AS 0584 upper limit. Though the sample is X-ray selected and suffers a bias against fainter objects, the discrepancy indicates the bright elliptical is not a cD galaxy located in a galaxy cluster.

4. DISCUSSION

An *ASCA* GIS observation of the region between A3391 and A3395 outlines a swath of excess X-ray emission connecting A3395 to the galaxy group. The excess emission is aligned with the general direction of a filament as outlined by the alignment of the clusters MS 0620.6, A3391, and A3395 (Fig. 3). If the emission was the result of gas ejected from the A3395 system, which is double peaked in X-ray emission and likely at some stage of a merger, the gas would not preferentially align itself with the filament. A similar argument suggests against, but does not rule out, it being a result of a postimpact tidal tail between the A3395 system and the galaxy group. Hence, the excess emission is postulated to be from hot intercluster gas within the filament structure. Finally, the emission may have as its source the chance superposition of galactic gas. Without better spectroscopic information, the possibility cannot be ruled out. It is the spatial coincidence with the A3391-A3395 intercluster region and the alignment with the entire system that points to a relation with the system. It is likely, however, that some fraction of the emission may still be the result of intervening galactic gas. We are presuming that the fraction is small.

The flux rates from the filament gas, determined from the data from the various instruments as outlined in §§ 3.2.1 to 3.2.4, correspond to lower limits to the flux. The minimum fluxes, as listed in Table 3, are all consistent with a positive identification of excess flux but do not give an indication of what that flux might actually be.

Presuming a gas with a temperature of 1 keV and the intervening column density of hydrogen to be $n_H = 5.6 \times 10^{20}$ cm^{-2}, then for the common energy range 0.4–10 keV, the various instruments find the fluxes to be $(18 \pm 2) \times 10^{-13}$, $(12 \pm 2) \times 10^{-13}$, and $(5.5 \pm 0.8) \times 10^{-13}$ ergs cm^{-2} s^{-1} for the GIS, SIS, and PSPC detectors, respectively. The GIS and SIS fluxes include the correction for the 13% scattered light in the *ASCA* observations. The GIS and SIS data agree to within 3 σ, but the flux from the *ROSAT* PSPC data is $\frac{1}{3}$ to $\frac{1}{2}$ of the *ASCA*-derived fluxes. The discrepancy may be a result of the filament region being partially obscured by the support ribbing on both PSPC observations. The assumption of the gas having a temperature of 1 keV may also be at fault. The PSPC is progressively less sensitive to emission from hotter plasmas. If the temperature were 3 keV, for example, the flux inferred from the PSPC data would be 4 times greater, while that inferred from the SIS data would increase only marginally. It would double for the GIS data, however, which would not increase the agreement among the instruments.

The amount of material contained within the extended structure is difficult to ascertain since the density of the gas is not known and the emissivity is a strong function of density, going as ρ_g^2. Some estimates can be made, however, since the total luminosity goes as the volume emissivity, $\epsilon \propto T^{1/2}\rho_g^2$, multiplied by the total volume, $V = Al$. For a Mekal spectrum of a 1 keV gas, spanning the energy range 0.4–10 keV, the following relation is found:

$$F = \rho_g^2 \frac{V/\mathrm{Mpc}^3}{\mathrm{Dist}^2/\mathrm{Mpc}^2} 5.7 \times 10^{47} \text{ ergs cm}^{-2} \text{ s}^{-1} . \quad (5)$$

A flux of 21×10^{-13} ergs cm^{-2} s^{-1} corresponds to a luminosity of 1.3×10^{43} h_{65}^{-2} ergs s^{-1} in the range 0.4–10 keV.

The area of the region mask used to extract the fluxes from the observations is 311 $arcmin^2$ in area. At a recessional velocity of 15,500 km s^{-1}, this gives $A = 1.50$ h_{65}^{-2} Mpc^2. The ratio of the long axis to short is 1.6.

An upper limit may be found on the gas density by presuming that the emission is coming from a cylinder aligned perpendicular to the line of sight. If the cylinder has a diameter of 0.97 h_{65}^{-1} Mpc and length 1.55 h_{65}^{-1} Mpc, then its volume would be 1.2 h_{65}^{-3} Mpc^3. Such a volume gives a gas density of 3.7×10^{-28} $h_{65}^{-1/2}$ g cm^{-3} and $n_H = 1.7 \times 10^{-4}$ $h_{65}^{-1/2}$ cm^{-3}.

[10] http://archive.stsci.edu/cgi-bin/dss_plate_finder.

The description of the system laid out in § 2 implies that the system is tilted to the line of sight such that a distance projected on the sky spans a distance at least 6 times longer in depth with a range in inclination of 3°–9°. A cylinder 0.49 h_{65}^{-1} Mpc in radius and 4.2 h_{65}^{-1} Mpc in length tilted at 8° would project 1.5 h_{65}^{-2} Mpc^2 on the sky. Its volume would be 3.2 h_{65}^{-3} Mpc^3 and to create an equivalent emission would require a density of 2.6×10^{-28} $h_{65}^{-1/2}$ g cm^{-3} and $n_{\rm H} = 1.2 \times 10^{-4}$ $h_{65}^{-1/2}$ cm^{-3}. The total mass would be 1.2×10^{13} $h_{65}^{-7/2}$ $M_\odot$. The density corresponds to an overdensity of 800 $h_{65}^{-1/2}$ in the baryon content (assuming $\Omega_b = 0.04\ h_{65}^{-2}$), on the order of 100 times larger than expected for filaments. For a given observed flux and the relation, equation (5), the inferred density goes as $\rho \propto L^{-1/2}$, where L is the length of the cylinder. The minimum possible value for the inclination, 3°, gives an increase in the cylinder length sufficient to lower the inferred density by a factor of 1.6.

The derived characteristics for the intercluster gas are similar to those of the system described by Kull & Böhringer (1999). The total mass of the filament given by the previous estimate is 1.7% $h_{65}^{-5/2}$ of the total mass of the system (presuming a total mass of 7×10^{14} h_{65}^{-1} $M_\odot$; Henriksen & Jones 1996) and 12% $h^{-5/2}{}_{65}$ of the total gas mass of the system (1×10^{14} h_{65}^{-1} $M_\odot$; Henriksen & Jones). Kull & Böhringer find the intercluster gas comprises 5% of the total system mass. The luminosity is $\frac{1}{3}$ of that described by Kull & Böhringer. The estimated density translates into an electron density of $n_e = 1 \times 10^{-4}$ $h_{65}^{-1/2}$ cm^{-3}, which is twice the value found in the Shapley supercluster. Given the sensitivity of these estimates to the presumed geometry, it is possible that they are the same class of object.

It would be expected that the search for filamentary gas would first find the high density tail in the distribution. Hence, the high apparent gas densities of these systems should not exclude them as candidates for filamentary gas.

The flux surface brightness is 6×10^{-15} ergs cm^{-2} s^{-1} arcmin^{-2} (0.4–10 keV). The surface brightness is more than 30 times larger than that for the filament report in Scharf et al. (2000), which has a flux more in line with expectations for filamentary gas as seen in numerical simulations (Cen & Ostriker 1999), although their detection is only at the 3 σ level.

The galaxy group has a flux of $(2.0 \pm 0.3) \times 10^{-13}$ ergs cm^{-2} s^{-1} (0.8–10 keV) measured by the GIS2 and GIS3 instruments. The corresponding luminosity is $(1.2 \pm 0.2) \times 10^{42}$ h_{65}^{-2} ergs s^{-1}. Its projected area (3′ at 260 Mpc) is 0.16 h_{65}^{-2} Mpc^2. Presuming it is spherical, that translates to a volume of 0.05 h_{65}^{-3} Mpc^3. Using the same assumption of a 1 keV gas, then equation (5) requires $\rho_g = 6.7 \times 10^{-28}$ $h_{65}^{-1/2}$ g cm^3 and a total gas mass of 4.9×10^{11} $h_{65}^{-7/2}$ $M_\odot$. This mass is about 4% of the mass for the intercluster gas.

In a survey of Hickson Compact Groups with the *ROSAT* PSPC, Ponman et al. (1996) find a range in $L_{\rm X}$ of 10^{41}–10^{43} h_{65}^{-2} ergs s^{-1}, with the spiral-dominated groups confined to less than 10^{42} h_{65}^{-2} ergs s^{-1}. Mulchaey et al. (1996) find for poor groups of galaxies a similar range but with the majority greater than 10^{42} h_{65}^{-2} ergs s^{-1}. In a comparison of 20 loose groups to 22 compact groups (from Ponman et al. 1996), Helsdon & Ponman (2000) find a luminosity span for the loose groups of 10^{41} to 5×10^{43} h_{65}^{-2} ergs s^{-1}, essentially indistinguishable from the compact groups. Hence, our measurement is consistent with classification as an early-type dominated compact group or a faint loose group. The group would be in the low-luminosity range for poor groups.

That the luminosity is consistent with a group of galaxies is significant, since the redshift data (described in § 2) demonstrate that the five principal galaxies are a chance alignment of at least two pairs of galaxies. For a single galaxy to be responsible for the emission, it would need to be a massive elliptical. No B magnitudes are available for the galaxies, but the Deep Sky Survey image indicates that none of the galaxies are particularly bright. The X-ray data demonstrates that there is at least one true group of galaxies but the resolution is not sufficient to attribute the emission to either the eastern or western pair of similar-redshift galaxies.

The galaxy distribution, as illustrated in Figure 1, shows a greater than 2 σ enhancement to the north of A3395 NW that coincides with the location of the excess X-ray emission as illustrated in Figure 4. The A3395 cluster and the galaxy group are sufficiently separated that the enhancement in the galaxy distribution is likely not a result of percolation of the contour line.

The temperature of the gas was not determined owing to the low number of counts. A temperature greater than 1 keV may be required to resolve the discrepancy between the *ROSAT* PSPC estimated flux and the *ASCA* GIS. A higher temperature would not be incompatible with the identification of the gas with filamentary material as suggested from numerical simulations since, as mentioned, selection effects dictate that the hottest, densest members of this postulated population would be found first.

The nature of the gas would be clarified if its temperature were known. Further observations, particularly using *XMM-Newton*, would help determine the state and extent of the gas. It is important to know if such emission truly does represent a population of dense, filamentary gas or is simply a by-product of local cluster activity.

This research has made use of data obtained through the High Energy Astrophysics Science Archive Research Center Online Service, provided by the NASA/Goddard Space Flight Center; the NASA/IPAC Extragalactic Database (NED) operated by the Jet Propulsion Laboratory, California Institute of Technology, under contract with the National Aeronautics and Space Administration; NASA's Astrophysics Data System Abstract Service; the *ROSAT* X-Ray All-Sky Survey archive at the Max-Planck-Institut für extraterrestrische Physik; and data retrieved through the Digitized Sky Surveys were produced at the Space Telescope Science Institute under U.S. Government grant NAG W-2166. The Second Palomar Observatory Sky Survey (POSS-II) was made by the California Institute of Technology with funds from the National Science Foundation, the National Geographic Society, the Sloan Foundation, the Samuel Oschin Foundation, and the Eastman Kodak Corporation.

The paper was improved significantly by the detailed comments of an anonymous referee.

We thank the National Science Foundation for support through grant AST 96-24716 and NASA for support through grant NASA NCC5-367-3.

REFERENCES

Abell, G. O., Corwin, H. G., & Olowin, R. P. 1989, ApJS, 70, 1
Bertin, E., & Arnouts, S. 1996, A&AS, 117, 393
Bond, J. R., Kofman, L., & Pogosyan, D. 1996, Nature, 380, 603
Bond, J. R. & Myers, S. T. 1996, ApJS, 103, 1
Briel, U. G., & Henry, J. P. 1995, A&A, 302, L9
Burns, J. O. 1990, AJ, 99, 14
Campos, A., Yahil, A., Windhorst, R. A., & Richards, E. A. 1999, ApJ, 511, L1
Cen, R. & Ostriker, J. P. 1999, ApJ, 514, 1
Churazov, E., Gilfanov, M., Forman, W., & Jones, C. 1996, ApJ, 471, 673
Colberg, J. M., White, S. D. M., Jenkins, A., & Pearce, F. R. 1999, MNRAS, 308, 593
De Grandi, S., et al. 1999, ApJ, 514, 148
Dickey, J. M., & Lockman, F. J. 1990, ARA&A, 28, 215
Donnelly, R. H., Forman, W., Jones, C., Quintana, H., Ramirez, A., & Churazov, E. 2001, Mergin Binary Clusters, preprint (astro-ph/0106482v3)
Fukugita, M., Hogan, C. J., & Peebles, P. J. E. 1998, ApJ, 503, 518
Fuller, T. M., West, M. J., & Bridges, T. J. 1999, ApJ, 519, 22
Gioia, I. M., Maccacaro, T., Schild, R. E., Stocke, J. T., Liebert, J. W., Danziger, I. J., Kunth, D., & Lub, J. 1984, ApJ, 283, 495
Gregorini, L., de Ruiter, H. R., Parma, P., Sadler, E. M., Vettolani, G., & Ekers, R. D. 1994, A&AS, 106, 1
Helsdon, S. F., & Ponman, T. J. 2000, MNRAS, 319, 933
Henriksen, M., & Jones, C. 1996, ApJ, 465, 666
Kull, A., & Böhringer, H. 1999, A&A, 341, 23
Lambas, D. G., Groth, E. J., & Peebles, P. J. E. 1988, AJ, 95, 996
Markevitch, M. 1998, ApJ, 504, 27
———. 1999, ApJ, 522, L13
Markevitch, M., Forman, W. R., Sarazin, C. L., & Vikhlinin, A. 1998, ApJ, 503, 77
Mulchaey, J. S., Davis, D. S., Mushotzky, R. F., & Burstein, D. 1996, ApJ, 456, 80
Peacock, J. A. 1999, Cosmological Physics (Cambridge: Cambridge Univ. Press)
Pierre, M., Bryan, G., & Gastaud, R. 2000, A&A, 356, 403
Ponman, T. J., Bourner, P. D. J., Ebeling, H., & Bohringer, H. 1996, MNRAS, 283, 690
Ptak, A., Serlemitsos, P., Yaqoob, T., Mushotzky, R., & Tsuru, T. 1997, AJ, 113, 1286
Ptak, A. F. 1997, Ph.D. thesis, Univ. Maryland College Park
Raymond, J. C., & Smith, B. W. 1977, ApJS, 35, 419
Renzini, A. 1997, ApJ, 488, 35
Scharf, C., Donahue, M., Voit, G. M., Rosati, P., & Postman, M. 2000, ApJ, 528, L73
Stocke, J. T., Morris, S. L., Gioia, I. M., Maccacaro, T., Schild, R., Wolter, A., Fleming, T. A., & Henry, J. P. 1991, ApJS, 76, 813
Struble, M. F., & Rood, H. J. 1999, ApJS, 125, 35
Teague, P. F., Carter, D., & Gray, P. M. 1990, ApJS, 72, 715
Tripp, T. M., Savage, B. D., & Jenkins, E. B. 2000, ApJ, 534, L1
Tritton, K. P. 1972, MNRAS, 158, 277
Tsusaka, Y., et al. 1995, Appl. Opt., 34, 4848
Wang, Q. D., Connolly, A., & Brunner, R. 1997, ApJ, 487, L13
Wright, A. E., Griffith, M. R., Burke, B. F., & Ekers, R. D. 1994, ApJS, 91, 111
Wright, A. E., & Otrupcek, R., eds. 1990, Parkes Catalogue (Parkes: Australia Telescope National Facility)